JOURNAL OF MATERIALS SCIENCE 30 (1995) 1087–1094

Low-temperature formation mechanism of double oxides $Fe_xZr(Ti)_{1-0.75x}O_{2-\delta}$ prepared from alkoxides and acetylacetonates

M. V. TSODIKOV, O. V. BUKHTENKO
Institute of Petrochemical Synthesis of Russian Academy of Sciences (RAS), Leninskii prosp., 29, Moscow, 117912, Russia

O. G. ELLERT, V. M. SHCHERBAKOV
Institute of General and Inorganic Chemistry of RAS Leninskii prosp., 31, Moscow, 117907, Russia

D. I. KOCHUBEY
Institute of Catalysis of Academy of Sciences, Siberian Branch, Acad. Lavrent'ev prosp., Novosibirsk, 630090, Russia

As a result of titanium and zirconium alcoholates hydrolysis in the presence of dissolved $Fe(acac)_3$, amorphous iron-containing gels have been synthesized. Their heat treatment has led to polycrystalline double oxides $Fe_xZr_{1-0.75x}O_{2-\delta}$ (C) and $Fe_xTi_{1-0.75x}O_{2-\delta}$ (T) formation. It has been shown that oxides (C) and (T) are likely to be solid solutions with $0.01 < x < 0.17$ and $0.01 < x < 0.14$, respectively. On the basis of X-ray diffraction and extended X-ray absorption fine structure data, iron–zirconium and iron–titanium crystallite models for gels and oxides have been proposed. It has been found that the crystallization process does not lead to a significant change in interatomic distances typical for local structures detected in gels.

1. Introduction

Much research dedicated to the development of the direct synthesis of complex metal oxides, which are widely applied in different fields of technology, has been carried out [1–3]. One of the promising advances in this field is sol–gel processing using metal alcoholates. However, sol–gel methods have a number of disadvantages (for instance, the instability of some alcoholates, the difficulties of their synthesis, and their different hydrolysis rates in the course of alkoxo-synthesis). At the same time, one of the significant advantages of these methods is the fact that multicomponent, single-phase metal oxides can be formed at relatively low temperatures in comparison with solid-phase reaction. For example, it is impossible to obtain single-phase compounds by the solid-phase reaction between ZrO_2 and TiO_2 at temperatures up to 1300 °C [4].

It was shown previously [5, 6] that metal-containing gels are products of the aluminium, titanium, zirconium alcoholate hydrolysis with the group VIII transition metal acetylacetonates solutions. The heat treatment of gels leads to single-phase metal oxides formation even at 500 °C [5, 6]. Therefore, careful study of the formation of these compounds, including the gel stage, is of interest. In this paper we discuss magnetic properties and the structure of iron-containing titanium and zirconium gels obtained by the reaction mentioned above and the double oxides which have been formed from these gels.

2. Experimental procedure

The basic reagents were $Fe(acac)_3$ obtained by electrolysis [7] and titanium(IV) isobutylate and zirconium(IV) isopropylate were used. Absolute benzene was used as a solvent. The titanium- and zirconium-alcoholate hydrolysis was performed with $Fe(acac)_3$ in 80% boiling ethanol. At the end of the hydrolysis the synthesized gel was separated from the mother liquer by centrifuging, dried in air at room temperature and then under vacuum at 50 °C. The oxide compounds were formed by heat treatment at 500 °C for 6 h.

The X-ray diffraction analysis was performed with a powder diffractometer using FeK_α radiation. The lattice type and unit cell parameters were determined by the procedure described elsewhere [8].

The static magnetic susceptibility was measured using a home-made Faraday-type magnetic balance [9] in the temperature range 77–570 K.

The composition of the gels and the metal oxides was determined by the atom-absorption spectrometry method using a Perkin–Elmer spectrometer.

The extended X-ray absorption fine structure (EXAFS) Zr-, Fe-, Ti-edges spectra were registered on

0022–2461

EXAFS station of Sibirian Center of SR Storage ring VEPP-3, which operated with an electron beam energy of 2 GeV and an average current stored of 70 A. Data were collected using a cut Si (1 1 1) crystal monochromator. Harmonics rejection for Ti-, Fe-edges was produced by total reflection by a silver mirror installed in the monochromatic beam. Harmonics rejection for the Zr-edge (18 keV) was not necessary, because the third harmonic (54 keV) is not present in the storage ring emission spectrum. Data were obtained in transmission mode with a step of 2 eV. Ion chambers filled up to 1 atm with argon (full adsorption) or 5% Ar + 95% He (monitoring) were used as detectors. Energy resolution was estimated to be about 1.5 eV by the use of an α-Fe_2O_3 pre-edge feature. The samples were prepared in the form of pellets by mixing powder with a small amount of apiezon as a binder. The pellet thickness was varied to obtain the adsorption jump $\Delta\mu_x = 0.8$ for the measured absorption edge. Total adsorption was not more than 3. The powder fraction did not exceed 0.05 mm. The spectra measurements were performed in air. The oscillating part of the absorption spectra, $\chi(k)$, was extracted by a standard procedure [10]. The pre-edge region was extrapolated to that of, EXAFS with polynomes of Victoreen type. The smooth part of the absorption coefficient was constructed with three interpolation cubic splines. In addition, the remains of the smooth part were removed by smoothing splines. $\chi(k)$ was normalized on the difference between the smooth part of the absorbtion coefficient and the background absorbtion. The inflection point on the absorbtion edge was used as the initial point E_0 ($k = 0$). Data analysis was made from the amplitude, $\rho(R - \delta)$, of Fourier transformation $k^3\chi(k)$ in the wave number interval 25–115 nm^{-1}. α-Fe_2O_3 anatase-type TiO_2 and cubic ZrO_2 + 10% Y_2O_3 oxides were used as model compounds with known structure [11]. The structural data were obtained by a curve-fitting procedure [12, 13] for Fe–Zr systems and by comparison of the radial distribution function (RDF) of atoms in unknown compounds with that for model compounds for the Fe–Ti system. Phase shifts, δ, were determined in the last case from EXAFS spectra for model compounds.

3. Results and discussion

Stained gels were synthesized in titanium and zirconium alcoholates hydrolysed in the presence of dissolved $Fe(acac)_3$. As pointed out [5, 6], their colour intensity was enhanced with increase of the basic components concentration. The elementary composition analysis and infrared spectroscopy data indicated [5, 6] that the chelate organic part, as well as metal, are incorporated into the gel.

Fig. 1 shows the dependence of the iron concentration in the gel on the ratio of basic reagents $n = Fe(acac)_3/M(OR)_4$, where M = Ti (IV) or Zr (IV). The initial curve up to mole ratio 0.3 is characterized by a steep gradient; with $n > 0.3$ the dependence became less.

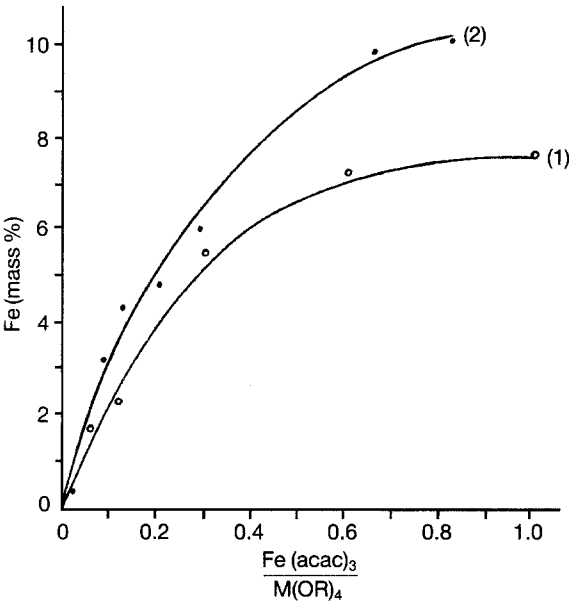

Figure 1 The dependence of iron concentration in the gel on the basic reagents ratio $n = Fe(acac)_3/M(OR)_4$, where M = Ti (IV) or Zr (IV). (1) Iron–zirconium gel, (2) iron–titanium gel.

X-ray analysis data have showed that iron-containing gels were amorphous. After heat treatment at 500 °C for 6 h, gels lost water and organic fragments and crystallized. In Tables I and II composition data and structural and magnetic characteristics of polycrystalline double oxides are presented. It can be seen from the tables that single-phase metal oxides are formed during heat treatment of gels in the range $0 < n < 0.3$. XRD analysis data indicate that they are likely to be solid solutions with empirical formula $Fe_xZr_{1-0.75x}O_{2-\delta}$ (C) with $0.01 < x < 0.17$, and $Fe_xTi_{1-0.75x}O_{2-\delta}$ (T) with $0.01 < x < 0.14$. In the above concentration limits, Vegard's law is valid.

It should be noted that reflex broadening for the 5C-sample with $x = 0.17$ was observed. Analysis of the influence of the different factors on diffraction line broadening has shown that it is caused by a coherent scattering region, block dispersivity and crystal lattice micro-distortions.

X-ray patterns of T-samples with $0 < x < 0.11$ were identified as anatase-type TiO_2 lattice [10, 11]. In contrast, the 6T-sample X-ray pattern is characterized by the appearance of the rutile phase and practically complete disappearance of the anatase phase.

Figs 2 and 3 show the inverse magnetic susceptibility dependence on temperature in the interval 77–570 K for a number of metal oxides (C, T). A $\chi^{-1}(T)$ experimental curve was satisfactorily described by the traditional Couri–Weiss law $\chi = C/T - \theta$ with the help of the best approximation program according to the method described elsewhere [9]. For samples 2C–6C (Fig. 2) and 3T, 4T, 6T (Fig. 3). The obtained Weiss constants, θ, were negative. Absolute θ values for oxides being formed in Fe–Zr–O system increased proportionally with x (as shown in Fig. 2b). Couri constants C for 2C–4C samples (Fig. 2) and 3T, 4T (Fig. 3) approximately corresponded to the high spin state of Fe^{3+} ions (electron configuration d^5,

TABLE I Structure characteristics and magnetic properties of iron–zirconium oxides

	Sample	Treatment temperature (°C)	Fe Content (wt %)	Type of crystal structure, a (nm)	Effective magnetic moment (BM)		C ($cm^3\ K\ mol^{-1}$)	θ (K)
					290 K	77 K		
1C	ZrO_2	500	0	Heterogeneous				
2C	$Fe_{0.05}Zr_{0.96}O_{2-\delta}$	500	2.3	Cubic 0.502	5.36	4.14	4.66	− 88.7
3C	$Fe_{0.06}Zr_{0.95}O_{2-\delta}$	500	3.1	Cubic 0.506	5.76	4.25	5.09	− 92.0
4C	$Fe_{0.13}Zr_{0.90}O_{2-\delta}$	500	6.1	Cubic 0.504	5.75	4.16	5.28	− 153.0
5C	$Fe_{0.17}Zr_{0.87}O_{2-\delta}$	500	7.9	Cubic 0.504	4.76	3.34	4.46	− 171.0
6C	$Fe_{0.25}Zr_{0.81}O_{2-\delta}$	500	11.8	Amorphous	4.27	3.05	3.88	− 186.0

TABLE II Structure characteristics and magnetic properties of iron-titanium oxides

	Sample	Treatment temperature (°C)	Fe content (wt %)	Type of crystal structure		Effective magnetic moment		C ($cm^3\ K\ mol^{-1}$)	θ (K)
				a (nm)	c (nm)	290 K	77 K		
1T	TiO_2	500	0	Tetragonal 0.376	0.944	–	–	–	
2T	$Fe_{0.01}Ti_{0.99}O_{2-\delta}$	500	0.6	Tetragonal 0.377	0.944	–	–	–	
3T	$Fe_{0.08}Ti_{0.94}O_{2-\delta}$	500	5.0	Tetragonal 0.377	0.943	4.31	3.80	4.91	−43.1
4T	$Fe_{0.09}Ti_{0.93}O_{2-\delta}$	500	7.1	Tetragonal 0.377	0.937	4.71	3.75	3.23	−95.1
5T	$Fe_{0.14}Ti_{0.90}O_{2-\delta}$	500	9.8	Tetragonal			–	–	–
6T	$Fe_{0.17}Ti_{0.87}O_{2-\delta}$	500	17.1	Heterogeneous			–	–	–

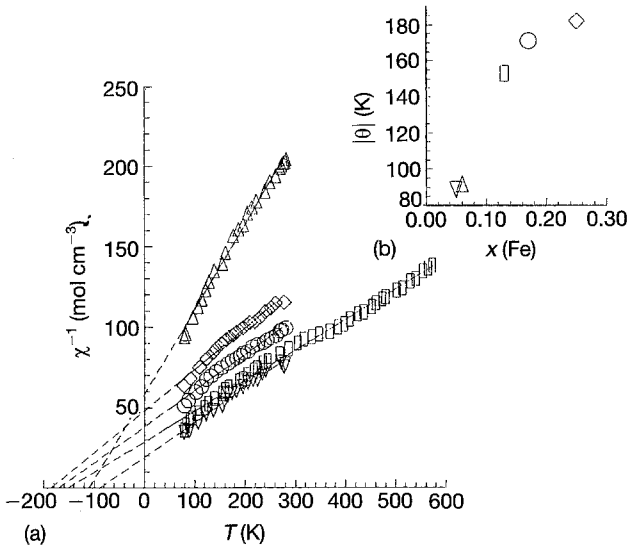

Figure 2 (a, b) The inverse molar magnetic susceptibility, χ^{-1}, dependence on temperature for the series $Fe_xZr_{1-0.75x}O_{2-\delta}$ (C) oxides. (▽) $Fe_{0.05}Zr_{0.96}O_{2-\delta}$, (△) $Fe_{0.06}Zr_{0.95}O_{2-\delta}$, (□) $Fe_{0.13}Zr_{0.90}O_{2-\delta}$, (○) $Fe_{0.17}Zr_{0.87}O_{2-\delta}$, (◇) $Fe_{0.25}Zr_{0.81}O_{2-\delta}$.

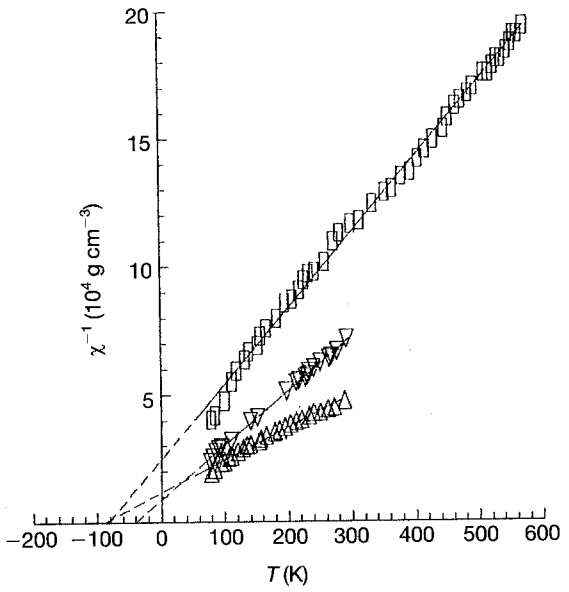

Figure 3 The inverse magnetic susceptibility, χ^{-1}, dependence on temperature for the series $Fe_xTi_{1-0.75x}O_{2-\delta}$ (T) oxides. (▽) $Fe_{0.08}Ti_{0.94}O_{2-\delta}$, (□) $Fe_{0.09}Ti_{0.93}O_{2-\delta}$, (△) 17.1% Fe.

$S = 5/2$, Table I). These data are confirmed by Mössbauer spectroscopy data [6]. To describe the magnetic behaviour of given samples, Heisenberg hamiltonian for infinite chains and two dimensional layers with intermolecular interaction of Fe^{3+} ions was used [9]. The attempt failed. This result, as well as the absence of any $\chi^{-1}(T)$ curve peculiarities within the studied temperature limits allows us to suppose that in C- and T-samples, magnetic short-range order interactions occur in the $[-Fe-O-Fe-]_n$ structure fragments which are statistically disordered within the oxide framework.

Figs 4 and 5 give some characteristic dependences of susceptibility and magnetization, M, on the applied magnetic field, H, for samples from C-series and T-series. One can see that for C with $0.05 < x < 0.14$ and T with $x = 0.08$ and 0.09, $\chi(H)$ is linear at room temperature. Straight lines $M(H)$ tend to the origin of coordinates. Some non-linearity can be revealed in curves for C-samples with $x = 0.17$ and 0.25 at 77 K (Fig. 4). A clearly marked dependence of susceptibility on field is characteristic for non-single-phase 6T-sample with 17.1 mass % (Fig. 5). Thus it might be assumed that near the border of the solid-solution existence region, magnetic-ordered precursors have been formed. These are undetected in the X-ray patterns but identified in the $\chi(H)$ plots. These precursors are assumed to be superparamagnetic γ-Fe_2O_3 clusters, which lead to the observed amorphization with increase of iron concentration (Table I).

The anatase and rutile phases identified in T-oxides cannot account for the dependence of $\chi(T)$. So, as in the case of C-samples, we suggest the presence of fine dispersive magnetic-ordered γ-Fe_2O_3 clusters in the 6T-sample with 17.1 mass % Fe. It should be noted that the quantity of iron incorporated into the gel as a result of chemical reaction influences, to a large extent, the phase composition and magnetic homogenity of the C- and T-crystal oxides (as in the case of iron aluminium oxides studied elsewhere [5]). By changing this parameter, we have an opportunity to form a

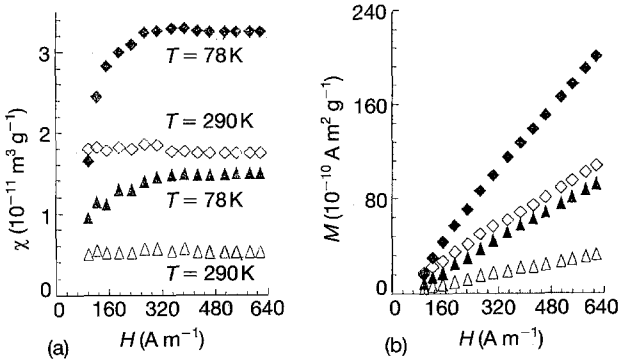

Figure 4 (a) Magnetic susceptibility, χ, and (b) magnetization, M, dependences on the applied magnetic field for the 2C sample ($x = 0.05$), (△) 290 K, (▲) 78 K, and 6C sample ($x = 0.25$), (◇) 290 K, (◆) 77 K.

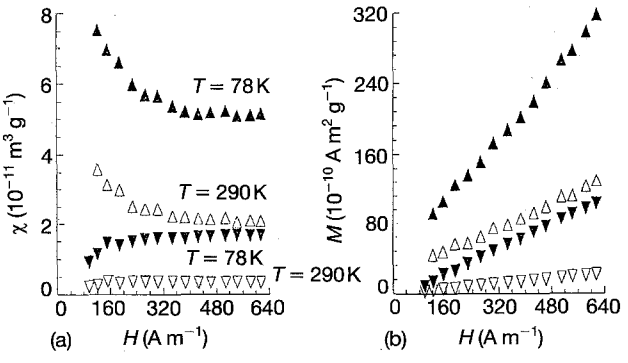

Figure 5 (a) Magnetic susceptibility, χ, and (b) magnetization, M, dependences on the applied magnetic field for the 3T sample ($x = 0.08$), (▽) 290 K, (▼) 77 K, and for the 6T sample ($x = 0.14$), (△) 290 K, (▲) 78 K.

relatively large solid-solution region in Fe–Zr–O and Fe–Ti–O systems at relatively low temperatures (500 °C). In these samples, in small crystalline block fragments, antiferromagnetic superexchange interactions between Fe^{3+} ions take place. Increase of the iron concentration in the gel up to 7.7 mass % in zirconium and 10.1 mass % in titanium samples, leads first to the formation of magnetically inhomogeneous samples in which ferrimagnetic highly dispersive γ-Fe_2O_3 phase precursors exist, as well as an antiferromagnetic phase, and then the amorphization structure.

In general, the evolution of gel structure and magnetic properties is likely to be similar to that for iron aluminium gels [14].

In order to study the structure of the gel in great depth, as well as the crystallization process, EXAFS was used.

To compare gels and oxides structure samples with close iron content, 4.2 mass % Fe in zirconium gel (sample 4C) and 4.3 mass % in titanium gel (sample 4T) and relative oxides (Tables I, II) were studied. The interatomic Fe–Zr distances obtained from the EXAFS spectrum were compared with distances in monoclinic ZrO_2 and in ZrO_2 + 10% Y_2O_3 with known cubic structure [11] which was prepared by the traditional solid-state reaction.

Fig. 6 shows initial Fe and Zr K absorbtion spectra and oscillating parts $k\chi(K)$ for gels and corresponding crystal oxides. Figs 7 and 8 demonstrate radial distribution functions of atoms (RDF) around iron and zirconium obtained by the treatment of oscillating spectrum parts in Fig. 6, as well as RDF of model ZrO_2 + 10% Y_2O_3. The results of the fitting procedure are presented in Table III. RDF around zirconium in the gel is characterized by two peaks. The first peak relates to the interatomic distance Zr–O with R = 0.215 nm and the second peak to Zr–Zr distance with $R = 0.349$ nm. The comparison of the RDF of the gel with the RDF of ZrO_2/Y_2O_3 reveals a shortening of the interatomic distances. The difference is also in the lower coordination number and greater Debye–Waller factor for Zr–Zr distance. One can suppose that the reason for these differences is the formation of small ZrO_2 polyhedra in the gel.

The RDF of atoms around iron in the gel is characterized by three interatomic distances. The first peak corresponds to an Fe–O distance with $R = 0.194$ nm, the second to Fe–Fe with $R = 0.312$ nm and the third to Fe–Zr with $R = 0.330$ nm.

The obtained data suggest that in pure zirconium gel, as well as in Fe–Zr gel, small clusters with a structure close to ZrO_2 form exist. Such clusters are connected by organic groups in the ZrO_2 gel and by iron ions in the octahedron environment for iron-containing gel.

In comparison with the gel RDF, the second peak intensity increase of the RDF curve around zirconium can be seen in crystal oxide 1C (Fig. 7d). Two basic interatomic distances Zr–O with $R = 0.214$ nm (first peak) and Zr–Zr with $R = 0.361$ nm (second peak) can be seen. Table III demonstrates that the Zr–Zr distance in iron-containing zirconium gel is shorter

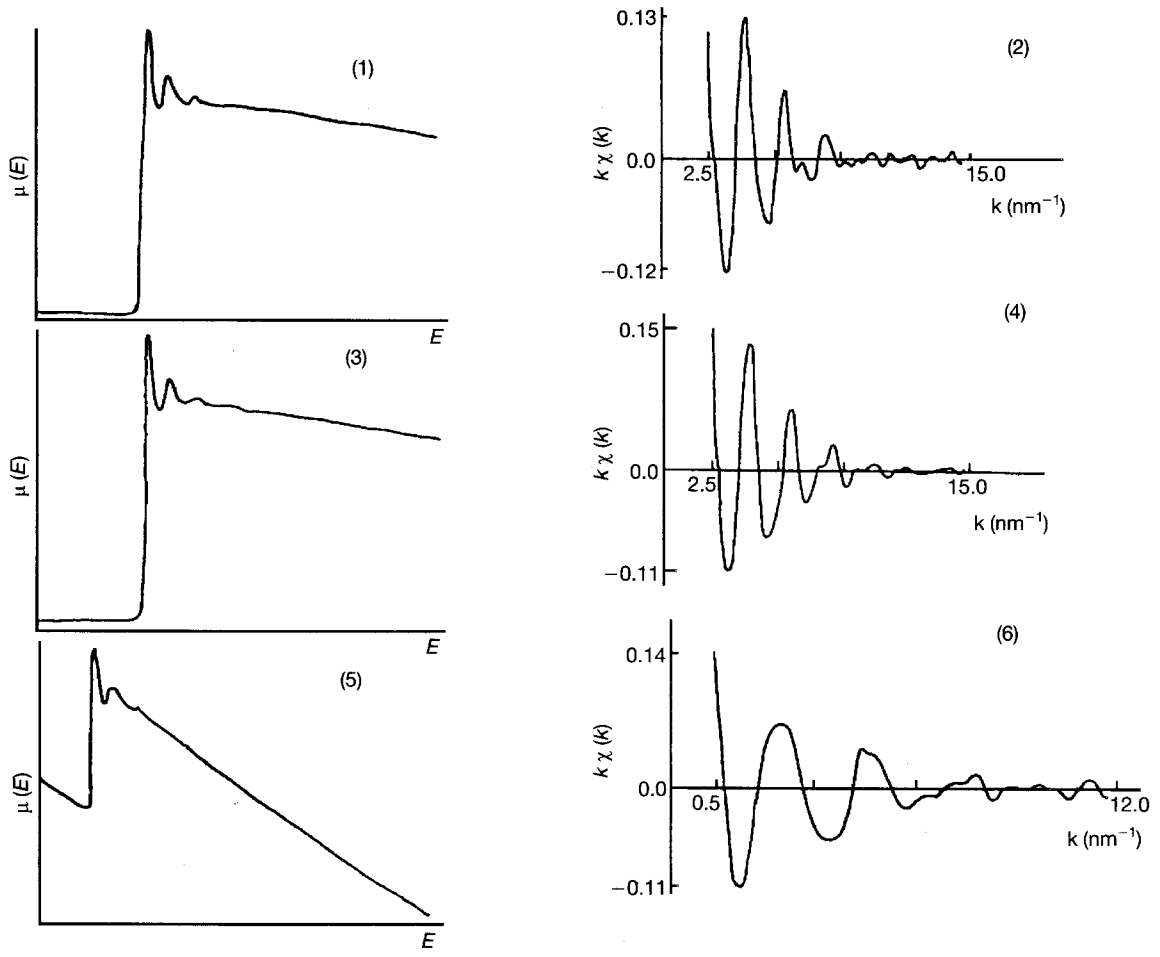

Figure 6 Absorption coefficient $\mu(E)X$ and oscillating part of absorbtion coefficient $k\chi(k)$ for zirconium in (1,2) ZrO_2 (500 °C), (3,4) gel $Zr(OH)_x(OR)_y$, and for iron in sample 4C (5, 6) $Fe_{0.13}Zr_{0.90}O_{2-\delta}$.

than that in ZrO_2 + 10% Y_2O_3. It should be also mentioned that the measured oxide interatomic distances are practically equal to that in the gel (Table III).

The insignificant changes in the RDF curves during sample crystallization, points to the fact that structure formation has already taken place in the gel. During crystallization, only extraction of organic fragments occurs, which contributes to the contraction of cubic polyhedra in the gel. This results in the appearance of cubic metal oxide with small structure distortion. Fe^{3+} ions are situated on the faces of the oxide and are epitaxial. Because of the large difference in the values of Zr–O and Fe–O distance, no more than one Fe^{3+} layer can exist on ZrO_2 face and the observed Fe–Fe distance (0.312 nm) appears to be the metal–metal bond between iron ions from different ZrO_2 clusters.

On the basis of the EXAFS data mentioned above, as well as magnetic susceptibility and XRD data the following model of the iron-containing zirconium oxide may be proposed (Fig. 9). In our opinion, it consists of crystal blocks of cubic ZrO_2, and Fe^{3+} ions produce epitaxial film on the face of the ZrO_2 cluster. Different ZrO_2 clusters are connected to each other by Fe^{3+} films.

Figs 10 and 11 show EXAFS oscillations and RDF functions around titanium and iron in a gel as well as in crystal oxide T with $x = 0.09$. It is necessary to emphasize that the RDF around titanium (Fig. 10) in an amorphous gel fully corresponds to the RDF of the model anatase-type TiO_2 [12]. Moreover Ti–Ti distances up to 0.6 nm can be seen easily. Because of the fact that six coordinating spheres for titanium environment can be seen in the RDF curves, and at least four can be seen for iron environment data, modulation was not performed because of the inefficient reliability of results which can be obtained by this method. Thus, Table IV shows only experimental data (peaks positions and intensity) as well as interatomic distances for model TiO_2, iron–titanium gel and $Fe_{0.09}Ti_{0.93}O_{2-\delta}$ oxide. These results are obtained with the use of crystallographic data and the EXAFS spectrum for anatase TiO_2. We have also taken into account the fact that experimental $R - \delta$ values corrections are practically similar for titanium and iron. The error in the interatomic distances determination in this case is more than for zirconium samples, but is in the region of 2% and does not exceed 4%. Hence, it is possible to say that within the limits of the experimental accuracy, the RDF curves for the titanium environment in the titanium samples fully correlate with the RDF curves for massive anatase. Moreover, the structure is well formed and distances up to 0.6 nm are observed. The RDF curves for the iron environment in studied samples 4T, partially coincide with one for titanium (peaks with $R - \delta = 0.270$ and

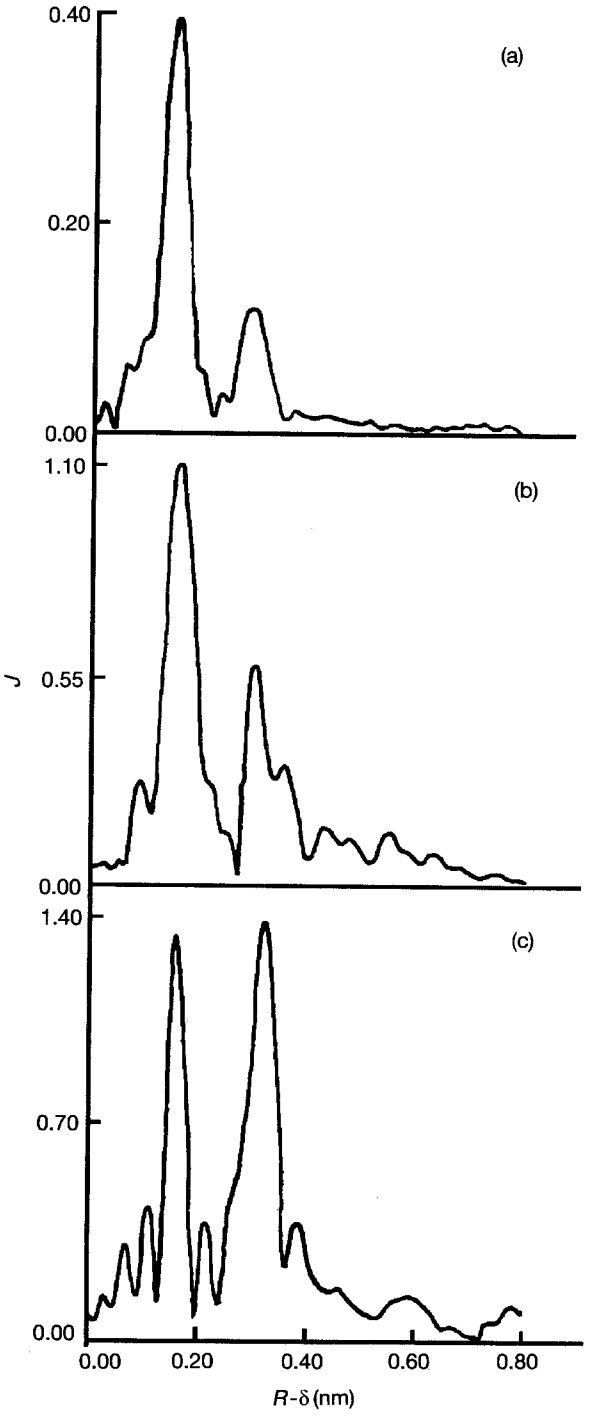

Figure 7 Radial distribution function (RDF) of atoms around zirconium (Fourier transformation $k^3\chi(k)$ in wavenumber interval 25–120 nm^{-1}) for (a) ZrO_2 gel, (b) sample 1C and (c) ZrO_2 + 10% Y_2O_3.

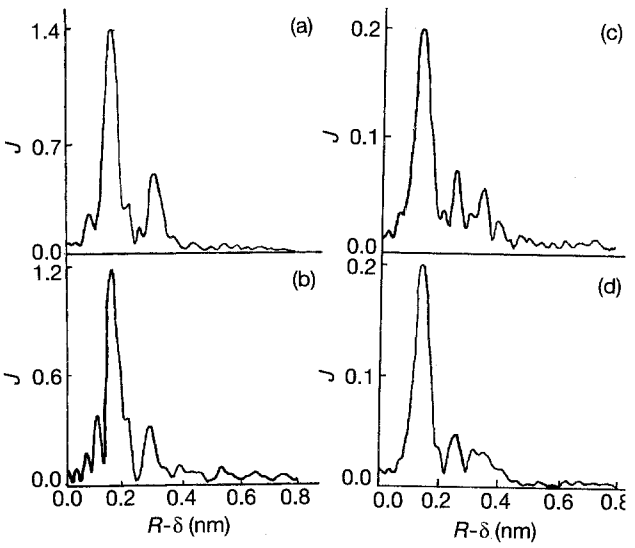

Figure 8 RDF of atoms around (a, c) zirconium ($k^3\chi(k)$, 25–120 nm^{-1}) and (b, d) iron ($k^2\chi(k)$, 25–120 nm^{-1}) for the sample 4C in (a, b) gel and (c, d) crystalline form.

TABLE III Basic structural parameters of gels and oxides prepared by sol-gel and solid phase reactions (EXAFS)

Zr interval, R, Å 0.9–4.15	ZrO_2 + 10% Y_2O_3	
	Zr–O	Zr–Zr
N	8.0	12.0
R, Å	2.16	3.66
$10^4\,\Delta\sigma^2$, Å	0	0
ΔE_0, ev	0	0
Zr interval, R, Å 0.9–4.2	ZrO_2 gel	
N	8.6	8.8
R, Å	2.15	3.49
$10^4\,\Delta\sigma^2$, Å	20	36
ΔE_0, ev	0.6	−6.0
Zr interval, R, Å 0.9–4.2	ZrO_2 oxide (500 °C)	
N	8.8	10.1
R, Å	2.14	3.61
$10^4\,\Delta\sigma^2$, Å	22	35
ΔE_0, ev	6.5	1.5

Zr,Fe interval R, Å 0.6–3.8, 0.9–4.3	Fe–Zr–O gel				
	Zr–O	Fe–O	Zr–Zr	Fe–Zr	Fe–Fe
N	9.2	6.5	8.2	3.8	2.6
R, Å	2.16	1.94	3.52	3.30	3.12
$10^4\,\Delta\sigma^2$, Å	9		24		
ΔE_0, ev	−2.6		−2.7		
Zr,Fe interval R, Å 0.9–4.2, 0.9–3.8	$Fe_{0.13}Zr_{0.9}O_{0.9}$ oxide				
N	9.2	8.0	8.2	4.5	3.0
R, Å	2.16	1.98	3.54	3.30	3.13
$10^4\,\Delta\sigma^2$, Å	24		26		
ΔE_0, ev	3.3		−3.6		

0.46 nm), but not fully. In particular, the 0.34 nm peak, which can be attributed to the main period of the lattice of anatase along the *a*-axis, is not observed. So it is concluded that iron ions are not incorporated in the TiO_2 framework, but that an Fe^{3+} ions epitaxial film exists on the face of the TiO_2 cluster, as in the case of the Fe–Zr–O system samples. As observed above, TiO_2 particles are mainly flattened along the *c*-axis and iron ions appear to stabilize on the (1 1 0) plane. The filling of the plane by iron ions is not complete, otherwise a distance of 0.38 nm would be observed.

However, we do not exclude the shift of iron ions from crystallographic positions of Ti^{4+} being caused by differences in oxygen coordination and leading to the appearance of two additional distances Fe–Ti 0.4 and 0.45 nm for gel and 0.38 and 0.43 nm for oxide.

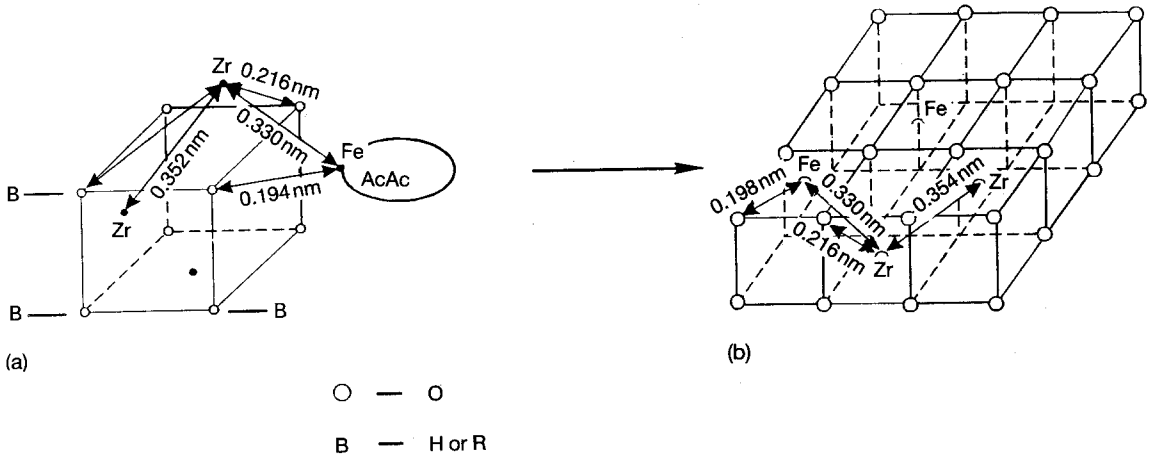

Figure 9 The model of the iron-containing zirconium gel and oxide.

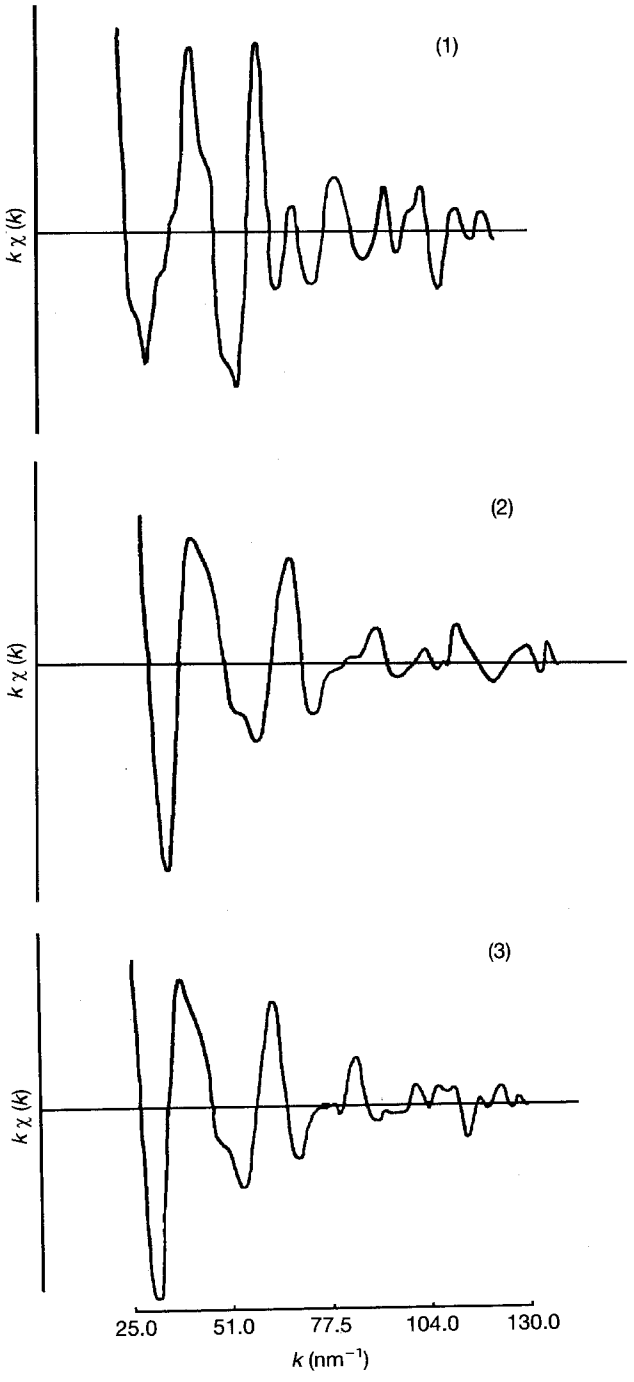

Figure 10 Oscillating part of absorption coefficient $k\chi(k)$ for (1) titanium in TiO_2 anatase-type, and (2) iron in gel 4T and (3) oxide $Fe_{0.09}Ti_{0.93}O_2$.

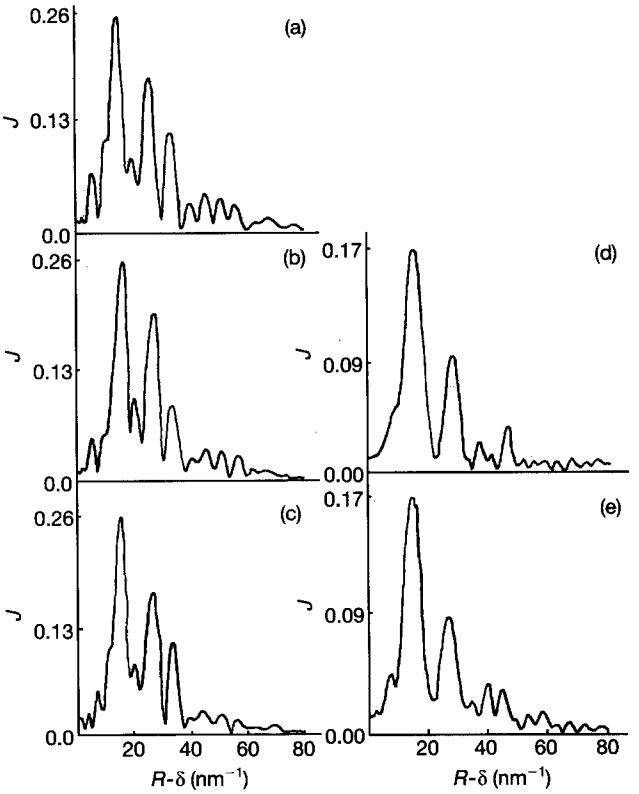

Figure 11 RDF of atoms around (a–c) titanium ($k^2\chi(k)$, 25–126 nm^{-1}) and (d, e) iron ($k^2\chi(k)$, 30–110 nm^{-1}) for (a) TiO_2 (anatase), (b, d) 4T gel sample, (c, e) 4T oxide $Fe_{0.09}Ti_{0.93}O_2$.

4. Conclusion

Amorphous iron-containing gels have been synthesized by titanium and zirconium alcoholates hydrolysis in $Fe(acac)_3$ solution. It has been demonstrated that in these gels polyhedra with interatomic distances typical of crystalline ZrO_2 and TiO_2 structures, are formed. Fe^{3+} ions stabilize the cubic structure in the iron–zirconium gel.

On the basis of XRD and EXAFS data, an iron–zirconium oxide crystallite model has been proposed. In accordance with this model crystallites are flattened cubic zirconium oxide clusters with a coherent scattering region of 10–12 nm. Iron ions are situated on the faces of these clusters.

TABLE IV Basic experimental EXAFS data for TiO_2 and Fe–Ti–O systems

TiO_2, anatas Type of bonds	R–δ, Å	J, abs	R, Å	$Fe_{0.09}Ti_{0.93}O_2$ Type of bonds	R–δ, Å	J, abs	R, Å	$Fe_{0.09}Ti_{0.93}O_2$ Type of bonds	R–δ, Å	J, abs
					gel				gel	
Ti–O	1.55	0.27	1.97	Ti–O	1.63	0.28	2.05	Fe–O	1.50	0.17
Ti–Ti	2.67	0.19	3.00	Ti–Ti	2.70	0.21	3.03	Fe–Ti	2.78	0.09
Ti–Ti	3.39	0.12	3.77	Ti–Ti	3.34	0.10	3.72	Fe–M*	3.72	0.02
Ti–Ti	4.58	0.05	4.84	Ti–Ti	4.53	0.04	4.79	Fe–M	4.12	0.01
Ti–Ti	5.12	0.04	5.33	Ti–Ti	5.02	0.04	5.23	Fe–M	4.60	0.04
Ti–Ti	5.64	0.03	6.06	Ti–Ti	5.62	0.03	6.04			
					oxide				oxide	
				Ti–O	1.55	0.25	1.97	Fe–O	1.50	0.17
				Ti–Ti	2.68	0.16	3.01	Fe–Ti	2.70	0.09
				Ti–Ti	3.38	0.10	3.76	Fe–M	3.47	0.03
				Ti–Ti	4.39	0.03	4.65	Fe–M	3.99	0.04
				Ti–Ti	5.08	0.03	5.29	Fe–M	4.53	0.03
				Ti–Ti	5.62	0.02	6.04			

* Where M–Fe, Ti.

In iron–titanium gel EXAFS spectra, one can observe the long-range order anatase-type TiO_2 structure. Oxide crystallization process does not lead to a significant change in interatomic distances, typical for structures detected in gels.

The amount of iron included into the gel appears to be the main, and the only, factor which determines the phase composition of the crystal oxides formed from the gels. From gels with iron concentrations from 1.75–5.46 mass %, one can obtain single-phase double oxides $Fe_xZr_{1-0.75x}O_{2-\delta}$ characterized as solid solutions. In the case of iron–titanium gels with iron concentrations from 0.4–5.9 mass %, solid solutions of $Fe_xTi_{1-0.75x}O_{2-\delta}$ are obtained. These compounds are magnetically uniform and antiferromagnetic exchange interactions between Fe^{3+} ions are realized. An increase in iron concentration in the gels causes the formation of amorphous and multiphase products at 500 °C.

The main advantage of the studied chemical reaction is the formation of intermediates with clearly defined structural phase characteristics in the gels. It is this phenomenon that permits single-phase double oxides, which possess structural characteristics of the intermediates formed, to be prepared under low temperatures compared to those used in traditional ceramic technology.

Acknowledgement

The support of the International Science Foundation (MI 8000) is acknowledged.

References

1. S. SAKKA and K. KAMIAGO, *J. Non-Cryst. Solids* **42** (1980) 403.
2. D. C. BRADLEY, *Chem. Rev.* **89** (1989) 1317.
3. R. C. MEHROTRA, *J. Non-Cryst. Solids* **121** (1990) 1.
4. T. KAZUGUKI and U. YASUO, *J. Catal.* **102** (1986) 246.
5. M. V. TSODIKOV, G. F. IVANOVA, O. G. ELLERT, YU. V. MAKSIMOV, O. V. BUKHTENKO and B. A. ZASLAVSKII, *Rus. Acad. Sci. Bull. Dev. Chem.* **8** (1988) 1898.
6. M. V. TSODIKOV, O. V. BUKHTENKO, O. G. ELLERT, V. V. MARKEVICH, YU. V. MAKSIMOV and S. M. LOKTEV, *ibid.* **2** (1991) 295.
7. V. A. SHREIDER, E. P. TUREVSKAIA, W. I. KOZLOVA and N. YA. TUROVA, *ibid.* **8** (1981) 1687.
8. S. S. GORELIK, V. N. RASTORGUEV and YU. A. SKAKOV, "Roengenographic and electronooptic analysis. (Metallurgy, Moscow, 1970) p. 72.
9. V. T. KALINNIKOV and YU. V. RAKITIN, "Introduction to magnetochemistry" (Nauka, Moscow, 1984) p. 54.
10. D. I. KOCHUBEY, YU. A. BABANOV, K. I. ZAMARAEV, R. V. VEDRINSKII, V. L. KRAYZMAN, G. N. KULIPANOV, L. N. MAZANOV, A. N. SKRINSKII, V. K. FEDOROV, B. YU. HELMER and A. T. SHUVAEV, "Rentgenospectralnii metod isuchenia strukturii amorfniih tel: EXAFS-spectroscopia" (Nauka, Novosibirsk, 1988) p. 306.
11. K. SCHUBERT, "Kristallstructuren zweikomponentiger Phasen" (Springer, Berlin, 1964) p. 532.
12. B. F. ORMONT, "The structures of inorganic compounds". (Technika-Theoretüchesckaia Literatura. Moscow, 1950) p. 458.
13. J. V. SMITH (ed) ASTM 4-0477 (American Society for Testing and Materials, Philadelphia, PA, 1960).
14. YU. V. MAKSIMOV, V. V. MATVEEV, I. P. SUZDALEV, M. V. TSODIKOV and O. G. ELLERT, *Hyperfine interaction* **57** (1990) 1983.

Received 19 February 1993
and accepted 7 June 1994